Vibrational Overtone Spectroscopy of Phenol and Its Deuterated Isotopomers

Shun-ichi Ishiuchi

Chemical Resources Laboratory, Tokyo Institute of Technology, PRESTO/JST, Nagatsuta, Yokohama 226-8503, Japan

Masaaki Fujii*

Integrated Research Institute/Chemical Resources Laboratory, Tokyo Institute of Technology, Nagatsuta, Yokohama 226-8503, Japan

Timothy W. Robinson,† Benjamin J. Miller, and Henrik G. Kjaergaard*

Department of Chemistry, University of Otago, P.O. Box 56, Dunedin, New Zealand

Received: February 2, 2006; In Final Form: April 13, 2006

We have measured the OH- and OD-stretching fundamental and overtone spectra of phenol and its deuterated isotopomers under jet-cooled conditions using nonresonant ionization detection spectroscopy and vapor-phase infrared (IR) and near-infrared (NIR) spectra at room temperature using conventional and photoacoustic spectroscopy. The OH- and OD-stretching bands in the jet-cooled spectra are about 1−10 cm^{-1} wide and generally show a few Lorentzian shaped peaks. The bands in the room-temperature spectra have widths of 20−30 cm^{-1} and display clear rotational profiles. The band profiles in the jet-cooled spectra arise mostly from nonstatistical intramolecular vibrational redistribution (IVR) with specific coupling to "doorway" states, which are likely to involve CH- and CD-stretching vibrations. The transition dipole moment that determines the rotational structure is found to rotate significantly from the fundamental to the third overtone and is not directed along the OH(D) bond. We use these calculated transition dipole moments to simulate the rotational structure. We determine the rotational temperature in the jet-cooled spectra to be about 0.5 K. Anharmonic oscillator local mode calculations of frequencies and intensities of the OH- and OD-stretching transitions are compared with our measured results. The calculated intensities are in good agreement with the absolute intensities obtained from conventional spectroscopy and with the relative intensities obtained from the room-temperature laser spectroscopy.

Introduction

The importance of vibrational overtone excitation has been suggested in atmospheric chemistry.[1] It was suggested that under certain atmospheric conditions the photolysis of nitric acid could proceed from a vibrational overtone excited state. This would occur at dusk and dawn when the UV light necessary for photolysis based on an electronic excitation was limited.[2,3] Subsequently it was demonstrated that for peroxinitric acid the overtone excitation process was, in many environments, the major atmospheric loss process.[4,5] More recently, the photolysis of sulfuric acid was suggested to proceed in the atmosphere predominantly via OH-stretching vibrational overtone excitation.[6,7] In sulfuric acid the electronic excitation was highly unlikely as the required high energy UV photons were not present in the atmosphere in sufficient quantities to compete with the overtone process.[6,8−11]

Experimental efforts to use overtone excitations to drive dissociation processes date back to the 1980s.[12−16] With the rapid progress in laser technology, various kinds of laser-based reaction control have been proposed and attempted.[17−25] These attempts have had some success for small molecules; however, the nanosecond lasers employed lacked the time resolution required by the fast relaxation process in these larger molecular systems. Nowadays, ultrafast laser systems are readily available, and chirped pulse[26,27] and laser phase[28] control have had some success.

Investigation of reaction control by vibrational overtone excitation requires knowledge of basic spectroscopic information of overtones such as transition energies and intensities, as well as detailed information regarding intramolecular vibrational redistribution (IVR) processes from the higher excited vibrational states. Theoretical studies are nontrivial because of the need for anharmonic potentials to predict the vibrational energy levels and nonlinear dipole moment functions to provide even qualitatively accurate transition intensities.

The intensity of vibrational overtone transitions typically falls by an order of magnitude for each successive overtone, which means that sensitive spectroscopic techniques must be employed in experimental studies. Vibrational overtone spectra are often measured at room temperature using sensitive techniques such as photoacoustic and cavity ring-down spectroscopy, but the broad spectrum observed at ambient temperature makes it difficult to obtain definitive information on dynamic processes such as IVR. This problem can be overcome by recording the spectra in the low-temperature environment of supersonic jet expansions; however, a highly sensitive spectroscopic technique

* To whom correspondence should be addressed. E-mail: henrik@alkali.otago.ac.nz (H.G.K.), mfujii@res.titech.ac.jp (M.F.).

† Present address: Manchester Computing, University of Manchester, Manchester M13 9PL, U.K.

10.1021/jp060723q CCC: $33.50
Published on Web 05/19/2006

must be employed because of the low concentration of sample in jet-cooled conditions. One such technique is nonresonant ionization detected infrared and near-infrared spectroscopy (NID-IR/NIR).[29] The high sensitivity of NID spectroscopy has been demonstrated by the measurement of the first, second, and third overtone OH-stretching transitions in phenol, catechol, and aminophenol.[30−32] The advantage of vibrational overtone spectroscopy in jet-cooled conditions was demonstrated by the resolution of geometrically similar rotational isomers in the *m*-aminophenol spectra.[32]

The infrared spectrum of vapor-phase phenol was studied in detail by Evans,[33] Green,[34] and Bist[35] in the 1960s, and recent ab initio and density-functional theory calculations of the harmonic frequencies in phenol and phenol-d_1 (C_6H_5OD) have resolved controversies that remained regarding the assignments of several of the fundamental vibrations.[36−38] The vibrational spectroscopy of phenol in the NIR region has been investigated less thoroughly. Ishiuchi et al.[31] recorded the NID spectra of jet-cooled phenol-d_0 in the 3600−14000 cm^{-1} region and assigned the OH-stretching transitions in the regions corresponding to $\Delta v_{OH} = 1-4$. Broad bands due to CH-stretching transitions in the first overtone ($\Delta v_{CH} = 2$) were also observed, and some weaker bands were assigned to combinations involving OH-stretching and other fundamental vibrations. The room-temperature overtone spectrum of vapor-phase phenol-d_0 in the regions corresponding to $\Delta v_{OH} = 4$ and 5 was recorded with laser photoacoustic spectroscopy by Davidsson et al.,[39] and the integrated cross sections of the vibrational overtone transitions were estimated by a comparison with the overtones of HD.[40] The NIR spectrum of phenol and phenol-d_1 in the 3800−10500 cm^{-1} region has also been studied in carbon tetrachloride solution.[41,42] It was found that in solution the bandwidths of the CH- and OH-stretching transitions increased with increasing vibrational quantum number, and this broadening was attributed to IVR. In contrast, the NID spectrum of jet-cooled phenol-d_0 showed a narrowing of bandwidth in each successive OH-stretching overtone.[31] Recently, the IVR of the OH-stretching fundamental transitions of phenol-d_0, -d_1, and -d_5 (C_6D_5OH) have been found to rely on doorway states, with contrasting lifetimes of 80 and 14 ps for phenol-d_0 and -d_5, respectively.[43,44]

In the present study, we have measured the room-temperature conventional and intracavity laser photoacoustic spectra of vapor-phase phenol and also the NID spectra of jet-cooled phenol and its deuterated analogues phenol-d_1, phenol-d_5, and phenol-d_6. We interpret the OH(D)- and CH(D)-stretching overtone spectra in terms of a local mode model.[45] We calculate fundamental and overtone stretching frequencies and intensities with an anharmonic oscillator (AO) local mode model with dipole moment functions obtained from ab initio and density-functional theory calculations.[30,46,47]

Experimental Section

Supersonic Jet Experiments. The experimental setup for the NID-IR/NIR spectroscopy has been described elsewhere.[31] Briefly, the second and third harmonics of Nd^{3+}:YAG lasers (HOYA-Continuum Powerlite8010; Lumonics YM1200) were used to pump two dye lasers (Lumonics HD-500). The output of the second harmonic-pumped dye laser was differentially mixed with the fundamental or the second harmonic of the YAG laser in a $LiNbO_3$ crystal (Inrad) to produce tunable IR laser in the 4−1.2 μm region. An idler light of an OPO laser (Spectra Physics MOPO/Pro230) and the dye laser (LDS765, LDS751) were used for the 1200−900 and 790−710 nm regions, respectively. The typical power of the IR/NIR laser is 0.1−0.5 mJ in the 3 μm region, 1 mJ in the 1.5 μm region, 2.5 mJ in the 1 μm region, and 15 mJ in the 730 nm region. The laser duration is 6 ns, and the typical line width is less than 0.1 cm^{-1}. The output of the third harmonic-pumped dye laser (C540A) was frequency doubled by a KDP crystal to produce UV radiation (~1 mJ, 6 ns duration). The UV and IR/NIR lasers were coaxially introduced into a vacuum chamber and crossed a supersonic jet. The UV laser was delayed 50 ns with respect to the IR/NIR laser. Molecules vibrationally excited by the IR/NIR radiation were selectively ionized by the UV laser via a nonresonant two-photon excitation. The frequency of the UV laser was fixed to 290 nm (34 483 cm^{-1}) which is slightly higher than a half of the ionization potential (IP) of phenol-d_0 (68 628 cm^{-1}).[48] The cations produced were pushed into a detector chamber by a repeller at an appropriate voltage (typically 15 V/cm) and were detected by a channel multiplier (Murata Ceratron) through a quadrupole mass filter (EXTREL). The signal was amplified by a preamplifier (EG&E PARC 115) and integrated by a digital boxcar (EG&E PARC 4420/4422). The integrated signal was recorded by a personal computer as a function of the IR/NIR laser frequency. In NID, the laser power changes over the wavenumber regions, and consequently, band intensities are relative and can only be compared in narrow wavenumber regions.

In the case of phenol-d_0, the vapor above crystalline phenol (99% Junsei Chemical) at room temperature was seeded in He gas (3 bar), and the mixture was expanded into the vacuum chamber through a solenoid valve. Phenol-d_1 was prepared by dissolving phenol-d_0 in D_2O (99.9% Aldrich), followed by dehydration under vacuum. The mixture of phenol-d_0 and -d_1 was purified by vacuum sublimation. Similarly, a mixture of phenol-d_5 and -d_6 was prepared from a solution of phenol-d_6 (98% Aldrich) in H_2O. The NID spectrum of a specific isotopomer is obtained by mass separation of the generated ions with a quadrupole mass filter. The NID spectra were deconvolved into Lorentzian peaks with a linear baseline with the Igor Pro (version 3.16) curve-fitting program.

Vapor-Phase Room-Temperature Experiments. Crystalline phenol (99+% redistilled, Aldrich, or ultrapure, ICN) was dried over molecular sieves prior to use. The IR fundamental spectrum of phenol vapor was recorded on a Bruker Equinox 55 FTIR spectrometer equipped with a DTGS detector and KBr beam splitter. A multipass cell fitted with Infrasil quartz windows was used with an optical path length of 4.8 m. The vapor was transferred to the evacuated cell at 22 °C, a temperature at which the vapor pressure of phenol is 0.27 Torr. The spectrum was recorded at a resolution of 0.5 cm^{-1} and averaged over 20 scans. It was noted that for longer scans the signal intensity weakened, most likely owing to the phenol adsorbing to the cell walls.

The vibrational overtone spectra of phenol vapor in the regions corresponding to $\Delta v_{OH} = 2$ and 3 and $\Delta v_{CH} = 2$ and 3 were recorded with a Cary 5e UV−vis−NIR spectrometer at the University of Guelph. The wavenumber accuracy of the Cary 5e is between ±1 and ±6 cm^{-1} in the NIR region. The sample cell was a White variable path length cell fitted with BK7 Schott glass windows, with the path length set to 20.25 m. The spectra were recorded with a fixed spectral bandwidth of 1 nm at a temperature of 19 °C. At this temperature the vapor pressure of phenol is 0.20 Torr. Background scans were performed with an evacuated cell, and these were subtracted from the sample scans.

The integrated absorption intensities $\int A(\tilde{\nu})d\tilde{\nu}$ of the OH- and CH-stretching bands from the conventionally recorded spectra were obtained using the integration module in Grams/32 (version

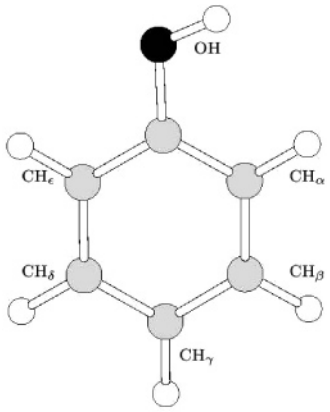

Figure 1. QCISD/6-311++G(2d,2p) optimized structure of phenol. The molecule is planar (C_s symmetry) with bond lengths (in Å) of OH = 0.9574, CH_α = 1.0829, CH_β = 1.0809, CH_γ = 1.0801, CH_δ = 1.0810, and CH_ϵ = 1.0802.

5.03). The integrated intensities were converted to oscillator strengths by

$$f = (2.6935 \times 10^{-9}\ \mathrm{K^{-1}\ Torr\ m\ cm})\frac{T}{pl}\int A(\tilde{\nu})\,\mathrm{d}\tilde{\nu} \quad (1)$$

where T is the temperature in K, p is the pressure in Torr, and l is the path length in m.

The room-temperature vapor-phase overtone spectra in the regions corresponding to $\Delta\upsilon_{OH} = 3-5$ and $\Delta\upsilon_{CH} = 4$ were recorded with intracavity laser photoacoustic spectroscopy (ICL-PAS). Our ICL-PAS setup has been described in detail previously.[49] The cell was filled with argon buffer gas at pressures of 180−200 Torr to increase the photoacoustic signal. Absolute intensities are not determined from our ICL-PAS spectra; however, accurate relative intensities can be obtained when several bands are accessible with the same set of optics. In the case of phenol, it was possible to obtain relative intensities of the $\Delta\upsilon_{OH} = 3$ and $\Delta\upsilon_{CH} = 4$ transitions and also of the $\Delta\upsilon_{OH} = 3$ and 4 transitions. Galactic Grams/32 (version 5.03) software was used for the integration.

Theory and Calculations

The dimensionless oscillator strength f of a transition from the ground vibrational state g to an excited vibrational state e is given by[47,50]

$$f = (4.702 \times 10^{-7}\ \mathrm{cm\ D^{-2}})\tilde{\nu}_{eg}|\vec{\mu}_{eg}|^2 \quad (2)$$

where $\tilde{\nu}_{eg}$ is the transition frequency in cm^{-1} and $\vec{\mu}_{eg} = \langle e|\vec{\mu}|g\rangle$ is the transition dipole moment in debye (D). The phenol molecule, as shown in Figure 1, has one OH oscillator and five nonequivalent CH oscillators. It has been shown that coupling between CH-stretching oscillators is generally only significant if the oscillators share a common heavy atom;[46,51] therefore, the CH- and OH-stretching overtone vibrations in phenol can, to a good approximation, be described as isolated nonequivalent local modes. Morse oscillators describe the wave functions of the XH-stretching modes, each with a local mode frequency $\tilde{\omega}$ and anharmonicity $\tilde{\omega}x$.

The dipole moment function (DMF) of each of the local modes is approximated as a series expansion in the internal stretching displacement coordinate with expansion coefficients determined from an ab initio calculated one-dimensional dipole moment curve. The dipole moment is calculated at nine points by stretching and compressing the bond from its equilibrium value in steps of 0.05 Å to a maximum displacement of ±0.2 Å.[52]

We have calculated one-dimensional dipole moment functions for the OH bond in phenol using the self-consistent-field Hartree−Fock (HF), quadratic configuration interaction including single and double excitations (QCISD), and Becke3−Lee−Yang−Parr (B3LYP) levels of theory all with the 6-311++G(2d,2p) basis set. The QCISD calculations required read−write files of about 50 Gb. Dipole moment functions for each of the CH bonds were calculated only with the HF and B3LYP methods.

For the OH or OD oscillator we have obtained the local mode parameters ω and $\tilde{\omega}x$ from a least-squares fit of the experimentally observed (NID) local mode peak positions $\tilde{\nu}$ to a two-parameter Morse oscillator energy expression

$$\tilde{\nu}/\upsilon = \tilde{\omega} - (\upsilon + 1)\tilde{\omega}x \quad (3)$$

In the CH-stretching regions it has not been possible to identify isolated transitions, and we have determined the local mode parameters from ab initio calculated anharmonic potential energy curves along the CH-stretching coordinates.[52] To compensate for deficiencies in the ab initio calculated potentials, we have scaled the calculated ω and $\tilde{\omega}x$ values with scaling factors determined by a comparison of calculated to experimental $\tilde{\omega}$ and $\tilde{\omega}x$ values in benzene.[53] We fitted the wavenumbers of the observed band maxima of the $\upsilon = 1-10$ CH-stretching transitions in benzene to eq 3 and obtain $\tilde{\omega} = 3159.7 \pm 0.9$ cm^{-1} and $\tilde{\omega}x = 57.37 \pm 0.14$ cm^{-1}, where the uncertainty is 1 standard deviation. With the B3LYP/6-311++G(2d,2p) method, this leads to scaling factors of 0.9907 and 0.8661 for $\tilde{\omega}$ and $\tilde{\omega}x$, respectively.

All ab initio and DFT calculations were performed with Gaussian 98.[54] The "tight" convergence criteria were used for geometry optimizations and self-consistent-field calculations, and dipole moments were calculated as analytical derivatives of the energy. The B3LYP calculations used the default integration grid size (FineGrid) with the Becke weighting scheme. Harmonic frequencies were calculated with the HF and B3LYP methods, and the B3LYP frequencies and oscillator strengths are given as Supporting Information in Table 1S.

The OD-stretching vibrations in the deuterated phenols are treated similarly to the OH-stretching vibrations. Within the Born−Oppenheimer approximation, the calculated DMF is identical for OH and OD bonds. The change in reduced mass leads to changes in the local mode parameters and consequently affects the transition dipole moment matrix elements.

Results and Discussion

Optimized Geometry. A planar geometry for phenol has been determined experimentally by microwave spectroscopy,[55] rotationally resolved fluorescence spectroscopy,[56] and electron diffraction,[57] as well as theoretically with a range of ab initio theories such as HF, MP2, and DFT. The QCISD/6-311++G(2d,2p) optimized geometry of phenol in the electronic ground state is shown in Figure 1 with the calculated bond lengths of the CH and OH oscillators given in the caption. The HF, B3LYP, and QCISD calculated CH and OH bond lengths are given as Supporting Information in Table 2S, and the full QCISD/6-311++G(2d,2p) geometry is given in Table 3S. The QCISD calculated OH bond length of 0.957 Å compares well with the experimental values of 0.956 Å from microwave data and 0.958 Å from electron diffraction.[55,57] The B3LYP value is in reasonable agreement, at 4 mÅ longer, and not surprisingly

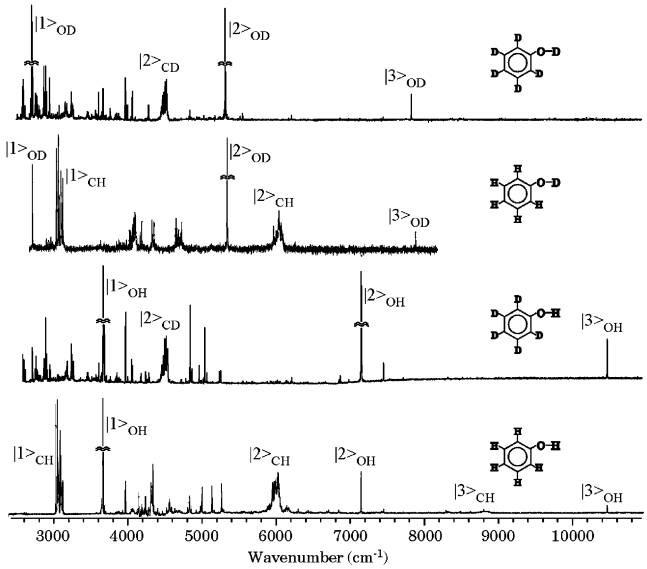

Figure 2. NID-IR/NIR overview spectra of jet-cooled phenol-d_0, phenol-d_1, phenol-d_5, and phenol-d_6.

the HF bond length is significantly shorter, by about 20 mÅ. The three methods give similar relative bond lengths for the five CH bonds in phenol with a spread of about 3 mÅ. The CH_γ and CH_ϵ bonds are of similar length to one another, as are the CH_β and CH_δ bonds, while the CH_α bond is significantly longer. One the basis of the similarity of the calculated CH bond lengths, we would not expect that the five individual CH-stretching transitions would be resolved in the room-temperature vapor-phase and jet-cooled spectra.

Jet-Cooled NID Spectra. In Figure 2 we present the NID overview spectrum of each of the jet-cooled phenol isotopomers. The spectra were obtained by mass-selecting the specific isotopomer (d_0, 94; d_1, 95; d_5, 99; d_6, 100) produced by the two-photon ionization. All peaks in the NID spectra correspond to vibrational transitions in the S_0 electronic ground state. The OH- and CH-stretching pure local mode transitions are increasingly dominant as the transition wavenumber increases. It is clear from the NID spectra that the band profile of the CH-stretching transitions is significantly wider than that of the OH-stretching transitions.

The NID spectrum of phenol-d_0 has been recorded and assigned previously.[31] The strong peak at 3656 cm^{-1} and a cluster of peaks around ~3000 cm^{-1} are assigned to the fundamental OH- and CH-stretching modes, respectively. In the 3700−5500 cm^{-1} region, peaks were generally assigned to combination bands involving one quantum of OH stretching and another fundamental vibration such as a ring mode.[31]

The overtones of the CH- and OH-stretching vibrations are easily assigned on the basis of vibrational frequency and intensity. The clusters of peaks around 6000 and 9000 cm^{-1} are assigned to the first overtone ($\Delta v_{CH} = 2$) and the second overtone ($\Delta v_{CH} = 3$) of the CH-stretching vibrations. The spectral profile of the CH-stretching regions is complicated both by the number of nonequivalent CH oscillators and by resonance coupling to lower frequency modes, in particular Fermi resonance between the CH stretching and bending modes. The sharp peaks at 7143, 10 461, and 13 612 cm^{-1} are assigned to the first, second, and third OH-stretching overtones, respectively.[31]

The OH-stretching transition wavenumbers observed in the NID spectrum compare well with those obtained from room-temperature measurements, as shown in Table 1. A fit of the observed NID wavenumbers to eq 3 led to the Morse oscillator

TABLE 1: Observed and Calculated OH-Stretching Frequencies (cm^{-1}) in Phenol-d_0

	observed			
v	NID	ICL-PAS	conventional	calcd[a]
1	3656		3656[b]	3655.9
2	7143		7142	7143.1
3	10461	10461	10460	10461.6
4	13612	13611[c]		13611.4
5		16595[c]		16592.5

[a] With the local mode parameters for phenol-d_0 in Table 2. [b] Davidsson et al.[39] reported a value of 3655 cm^{-1}. [c] Davidsson et al.[39] reported values of 13 611 and 16 590 cm^{-1} for the $\Delta v_{OH} = 4$ and 5, respectively.

TABLE 2: OH- and OD-Stretching Local Mode Parameters (in cm^{-1})[a]

	$\tilde{\omega}$	$\tilde{\omega}x$
phenol-d_0 (OH)	3824.6 ± 0.3	84.35 ± 0.1
phenol-d_5 (OH)	3829.2 ± 3	85.85 ± 1
phenol-d_1 (OD)	2788.6 ± 0.3	44.84 ± 0.1
phenol-d_6 (OD)	2792.9 ± 2	46.17 ± 0.8

[a] Determined from a fit of the NID transitions in Tables 1, 3, and 4 to eq 3. Uncertainties shown are 1 standard deviation.

local mode parameters for the OH-stretching vibration given in Table 2. The excellence of the fit shows that the OH-stretching vibration is essentially uncoupled from other vibrations and has a potential that is well described by a Morse function. The last column in Table 1 shows the calculated Morse oscillator energies based on the determined local mode parameters. The maximum discrepancy between the Morse calculated transition wavenumbers and the experimentally observed wavenumbers is just 0.6 cm^{-1} for NID and 2.5 cm^{-1} for the ICL-PAS.

On the basis of the assignment for phenol-d_0, the sharp peaks observed at 3658, 7141, and 10459 cm^{-1} in the spectrum of phenol-d_5 are assigned to the $\Delta v_{OH} = 1$, 2, and 3 transitions, respectively. The frequencies of these transitions are shifted by at most 2 cm^{-1} from their values in phenol-d_0, which provides further experimental evidence that the coupling between the OH-stretching and other vibrations is relatively small and supports our use of an isolated local mode to describe the OH-stretching potential. The cluster of peaks at about 4500 cm^{-1} is assigned to the first overtone of CD-stretching vibration ($\Delta v_{CD} = 2$), based on its vibrational frequency and the similarity of the spectral profile to that of the $\Delta v_{CH} = 2$ band in the phenol-d_0 spectrum.

The NID spectrum of phenol-d_6 also shows the cluster of peaks located around 4500 cm^{-1} which is assigned to $\Delta v_{CD} = 2$, with the structure of this band being similar to that observed in the phenol-d_5 spectrum. The sharp bands at 2701, 5307, and 7826 cm^{-1} are readily assigned to the $\Delta v_{OD} = 1$, 2, and 3 transitions, respectively.

The NID spectrum of phenol-d_1 is assigned by comparison to the NID spectra of phenol-d_0 and -d_6. The sharp bands at 2699, 5308, and 7828 cm^{-1} are assigned to the $\Delta v_{OD} = 1$, 2, and 3 transitions, respectively, and the clusters of peaks around 3000 and 6000 cm^{-1} are assigned to $\Delta v_{CH} = 1$ and 2 transitions. The observed OH-stretching transition frequencies for phenol-d_0 and -d_5 are summarized in Table 3, and the OD-stretching transitions in phenol-d_1 and -d_6 are summarized in Table 4. The fitted local mode parameters for the OH- and OD-stretching modes in all isotopomers are given in Table 2.

The ratio of OH- and OD-stretching frequencies and anharmonicities in the phenol-d_0 and -d_1 pair and in the phenol-d_5

TABLE 3: Calculated and Observed OH-Stretching Frequencies (cm^{-1}) and Calculated Oscillator Strengths for Phenol-d_0 and Phenol-d_5[a]

	phenol-d_0		phenol-d_5	
v	$\tilde{\nu}$	f	$\tilde{\nu}$	f
1	3656 (3656)	7.93×10^{-6}	3657 (3658)	7.92×10^{-6}
2	7143 (7143)	6.87×10^{-7}	7143 (7141)	6.91×10^{-7}
3	10462 (10461)	2.84×10^{-8}	10457 (10459)	2.94×10^{-8}
4	13611 (13612)	1.59×10^{-9}	13600	1.66×10^{-9}
5	16593	1.34×10^{-10}	16570	1.43×10^{-10}

[a] NID experimental peak positions in parentheses. Oscillator strengths are calculated with the QCISD/6-311++G(2d,2p) dipole moment functions and local mode parameters from Table 2.

TABLE 4: Calculated and Observed OD-Stretching Frequencies (cm^{-1}) and Calculated Oscillator Strengths for Phenol-d_1 and Phenol-d_6[a]

	phenol-d_1		phenol-d_6	
v	$\tilde{\nu}$	f	$\tilde{\nu}$	f
1	2699 (2699)	4.40×10^{-6}	2701 (2701)	4.39×10^{-6}
2	5308 (5308)	2.65×10^{-7}	5309 (5307)	2.68×10^{-7}
3	7828 (7828)	7.75×10^{-9}	7825 (7826)	8.17×10^{-9}
4	10258	3.06×10^{-10}	10248	3.35×10^{-10}
5	12598	1.89×10^{-11}	12579	2.13×10^{-11}

[a] NID experimental peak positions in parentheses. Oscillator strengths are calculated with the QCISD/6-311++G(2d,2p) dipole moment functions and local mode parameters from Table 2.

and -d_6 pair is very similar. The lack of change in these ratios upon deuteration of the ring supports our assumption that the OH- and OD-stretching vibrations are essentially uncoupled from the CH (CD)-stretching and ring modes. The ratio of the frequencies is 1.3715 (1.3710), slightly lower than the theoretical expected value of 1.3736. This small difference is possibly due to the influence of the COH (D) bending modes. Sage has shown that the change in OH (OD) bond length upon vibrational excitation changes the zero-point vibrational energy of the bending modes.[58] This effect would be slightly larger for the OH-stretching modes than for the OD-stretching modes and thus lead to a frequency ratio that is slightly smaller than the theoretically expected ratio is in agreement with our observations.

Room-Temperature Spectra. We have recorded room-temperature vapor-phase spectra of phenol in the $\Delta v_{OH} = 1-5$ regions and $\Delta v_{CH} = 1-4$ regions with FT-IR, conventional long path length, and ICL-PAS spectroscopy. The observed OH-stretching peak positions are listed in Table 1.

The FT-IR spectrum in the fundamental region is presented in the Supporting Information (Figure 1S). For longer scans, it showed a broad feature around 3450 cm^{-1} indicative of hydrogen-bonded OH-stretching transitions and is likely a result of a small amount of phenol condensing on the windows. The photoacoustic spectra in the $\Delta v_{OH} = 4$ and 5 regions are similar to those presented previously and are shown in Figures 2S and 3S.[39]

In Figure 3, we show the conventionally recorded spectrum of vapor-phase phenol-d_0 in the 5500−10700 cm^{-1} region. The $\Delta v_{OH} = 2$ and 3, and $\Delta v_{CH} = 2$ and 3 transitions are the most intense features. Three weaker features are observed on the low-frequency side of the $\Delta v_{CH} = 3$ band at about 8300, 8480, and 8615 cm^{-1}. These bands are better resolved in the NID spectrum where it becomes apparent that the feature around 8300 cm^{-1} comprises two peaks at 8293 and 8314 cm^{-1}, and the other two bands are observed at 8486 and 8619 cm^{-1}. We assign these bands to combinations involving two quanta of OH-stretching and one quantum of another vibrational mode. This other vibrational mode is labeled in Figure 3 using the notation from Bist et al.[35] The lowest energy transition of these was previously observed in the spectrum of phenol-d_0 in CCl_4.[59]

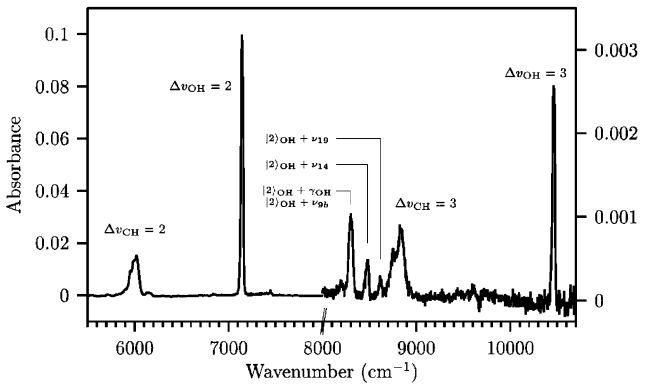

Figure 3. Conventional vapor-phase NIR spectrum of phenol-d_0. The spectrum was measured with a path length of 20.25 m at $T = 19$ °C where the pressure is ~0.2 Torr.

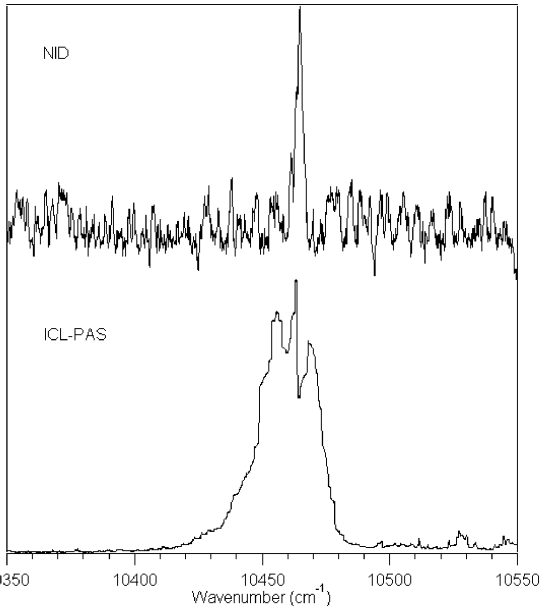

Figure 4. Jet cooled NID spectrum and room-temperature vapor-phase ICL-PAS spectrum of phenol-d_0 in the $\Delta v_{OH} = 3$ region.

The OH-stretching transitions show PQR rotational structure in the room-temperature spectrum. In Figure 4 we compare the spectrum of phenol-d_0 in the $\Delta v_{OH} = 3$ region at room temperature (ICL-PAS) and at jet-cooled conditions (NID). The full-width at half-maximum (fwhm) is 24 cm^{-1} in the ICL-PAS spectrum and 31 cm^{-1} in the conventional spectrum (not shown). The NID spectrum shows an approximately Lorentzian band shape with a fwhm of 2.8 cm^{-1}. The mechanisms relating to the line widths will be discussed later. The fwhm of the other OH-stretching transitions at ambient temperature are 27 cm^{-1} ($v_{OH} = 2$, conventional), 23 cm^{-1} ($v_{OH} = 4$, ICL-PAS), and 29 cm^{-1} ($v_{OH} = 5$, ICL-PAS).

OH- and CH-Stretching Band Intensities. The experimentally determined oscillator strengths of the OH-stretching transitions in phenol-d_0 are compared to those calculated with our anharmonic oscillator (AO) local mode model in Table 5. We have used the local mode parameters from Table 2 and three different ab initio dipole moment functions to calculate the transition oscillator strengths.

TABLE 5: Calculated and Observed Oscillator Strengths of the OH-Stretching Transitions in Phenol-d_0

v	experimental	HF[d]	B3LYP[d]	QCISD[d]
1	7.1×10^{-6},[a]	1.44×10^{-5}	7.85×10^{-6}	7.93×10^{-6}
2	5.7×10^{-7},[b]	6.15×10^{-7}	7.17×10^{-7}	6.87×10^{-7}
3	2.2×10^{-8},[b]	2.73×10^{-8}	3.60×10^{-8}	2.84×10^{-8}
4	1.6×10^{-9},[c]	1.64×10^{-9}	2.33×10^{-9}	1.59×10^{-9}
5	2.6×10^{-10},[c]	1.41×10^{-10}	1.58×10^{-10}	1.34×10^{-10}
6		1.74×10^{-11}	1.65×10^{-11}	1.66×10^{-11}

[a] From Etzkorn et al.[60] [b] This work, conventional spectrum. [c] From Davidsson et al.[39] [d] Calculated with the level of theory given and the 6-311++G(2d,2p) basis set. The local mode parameters in Table 2 have been used.

In the fundamental region we determined experimental oscillator strengths of 7.2×10^{-6} and 7.6×10^{-6} for the OH- and CH-stretching bands, respectively. Etzkorn et al. recently reported the OH-stretching fundamental intensity of phenol and other monocyclic aromatic hydrocarbons.[60] Their integrated cross section determined for the OH-stretching fundamental band in phenol was $(6.3 \pm 0.22) \times 10^{-18}$ cm molecule^{-1}, or an oscillator strength of $(7.1 \pm 0.25) \times 10^{-6}$, which is in excellent agreement with our present results, as well as in reasonable agreement with previous values of $(8.1 \pm 0.7) \times 10^{-6}$ and 7.8×10^{-6} determined in the 1960s by Broun[61] and Ingold,[62] respectively. Davidsson et al.[39] measured an integrated cross section of $(6.4 \pm 1.4) \times 10^4$ fm^2, with FTIR spectroscopy, which corresponds to an oscillator strength of $(2.6 \pm 0.6) \times 10^{-6}$ and is likely an underestimate of the true intensity. Their spectrum was acquired over a period of 1 h, during which some phenol may have adsorbed to the cell walls, resulting in an underestimated oscillator strength.[63]

The fundamental intensity has been calculated both with our anharmonic oscillator model, as detailed in the theory section, and also with the so-called double-harmonic approximation, which assumes harmonic potentials and linear dipole moment functions, within the Gaussian program.[54] As seen in Table 5, fundamental intensities calculated with the anharmonic oscillator model and QCISD or B3LYP dipole moment functions are within 10% of the experimental intensity. The HF calculated intensity is overestimated by a factor of 2, which shows the importance of electron correlation for an accurate prediction of fundamental intensities.[64] The double harmonic intensities are 1.88×10^{-5} and 1.16×10^{-5} for the HF and B3LYP calculation, respectively, or about 40% higher than the AO intensities with both levels of theory. The double harmonic B3LYP intensity is about 50% higher than the experimental value. This shows that the use of anharmonic oscillators in the vibrational model and inclusion of higher than linear terms in the dipole moment expansion are both important for the accurate prediction of fundamental intensities.

Davidsson et al. determined the experimental intensities of the $\Delta v_{OH} = 4$ and 5 transitions from the photoacoustic spectra by a comparison with overtone transitions in HD.[39] Their oscillator strength of 1.6×10^{-9} ($\pm 25\%$) for the $\Delta v_{OH} = 4$ transition is in good agreement with our estimated oscillator strength of 1.3×10^{-9}. Our estimate was made by comparing the relative intensities of the $\Delta v_{OH} = 3$ and $\Delta v_{OH} = 4$ bands measured in our ICL-PAS spectrum and the absolute intensity of the $\Delta v_{OH} = 3$ transition obtained from our conventional spectrum.

In Tables 3 and 4 we present the AO calculated frequencies and intensities of the OH- and OD-stretching transitions in the deuterated phenols. The observed and calculated frequencies agree well for all phenols, which again justifies the use of isolated Morse oscillators to describe the OH- and OD-stretching potentials. It is clear that the intensity of the OD-stretching transition drops off faster with increasing overtone compared to the OH-stretching transition, in agreement with the experimental observation shown in Figure 2 and the lower anharmonicity of the OD bond compared to the OH bond.

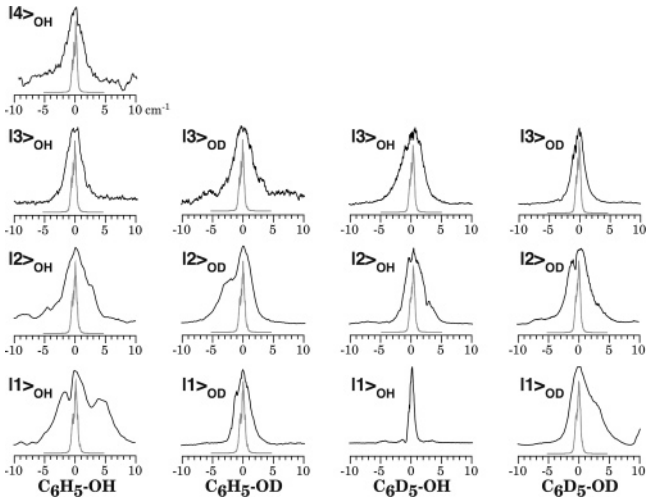

Figure 5. NID spectra of the OH- and OD-stretching transitions in jet-cooled phenol-d_0, phenol-d_1, phenol-d_5, and phenol-d_6 (black curves). Calculated band shapes (red curves) at 0.5 K are shown within the observed spectra.

The individual CH-stretching transitions and intensities have not been resolved, but we have measured the absolute intensity of the total CH-stretching region in phenol-d_0. These measured intensities agree reasonably well with CH-stretching intensities determined with the ab initio calculated and scaled local mode parameters (Table 4S). Relative intensities are easier to measure accurately than are absolute intensities. The relative intensity of the $\Delta v_{OH} = 3$ to $\Delta v_{CH} = 4$ transition is measured in our ICL-PAS spectrum to be about 8.4, which compares well with a calculated ratio of 10.7 at the HF level.

The agreement between the calculated and experimental intensities is very good for the overtones, which span several orders of magnitude. The addition of electron correlation in the dipole moment function leads to little or no improvement for the overtone transition intensities. This apparent insensitivity of overtone intensities to electron correlation has been noted previously for a number of molecules.[65−67]

OH- and OD-Stretching Bandwidths. The band profiles of each of the OH- and OD-stretching transitions of phenol-d_0, -d_1, -d_5, and -d_6 are shown in Figure 5. The calculated rotational profiles are shown as the lower curves. The calculation of rotational profiles will be discussed later. Despite the similar nature of the molecules a wide range of bands are observed with asymmetric profiles and widths in the 1−10 cm^{-1} range. The apparent three-peak structure in the $\Delta v_{OH} = 1$ band of phenol-d_0 is an artifact of a broad peak perturbed by IR laser power variations due to the absorption by atmospheric water, which could not be completely accounted for.

The origin of the bandwidth and shape is determined by a number of factors: the rotational structure (band type); the rotational temperature T_{rot} in the jet; the line broadening due to the relaxation such as intramolecular vibrational energy redistribution (IVR); and the line width of the IR laser. The line width of the IR laser is less that 0.1 cm^{-1} and thus much smaller than any of the observed bands and is not likely the main factor for the observed widths and shapes.

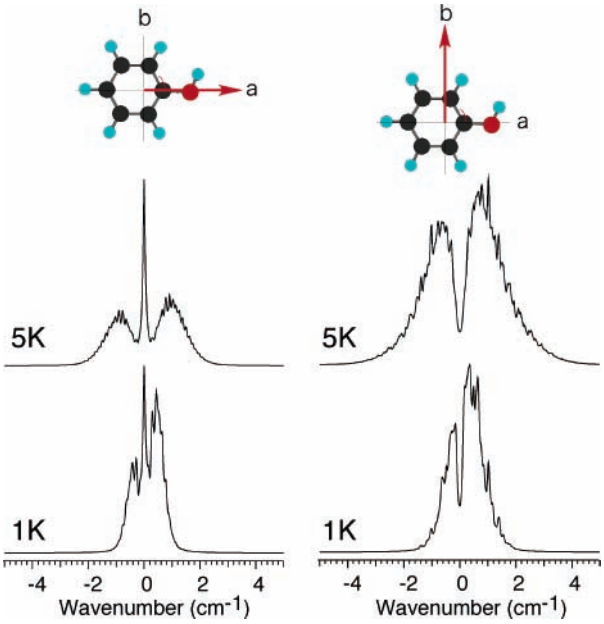

Figure 6. Calculated rotational contours for a pure a- and b-type rotational band in phenol-d_0, simulated at $T_{rot} = 1$ and 5 K for 0.1 cm^{-1} line widths of the individual rotational lines assuming Lorenztian line shapes.

We have simulated the theoretically expected rotational envelope. The *a* and *b* rotational axes of phenol-d_0 are shown with the molecule in Figure 6 and are very similar for the other isotopomers. The CO bond is almost parallel with the *a*-axis, whereas the OH bond lies largely along the *b*-axis. The rotational structure depends on the direction of the transition dipole moment (TDM) of the vibrational transition. If the TDM was simply along the OH bond, the rotational structure would be very close to b-type, in which the Q-branch is very weak and the band contour is split into separate P- and R-branches. However if the TDM was along the *a*-axis the rotational structure would be a-type and a strong Q-branch would be evident. In Figure 6 we show the simulated rotational band structure for an a- and b-type band, respectively, simulated at 1 and 5 K with individual rotational transitions having a line width of 0.1 cm^{-1} and a Lorentzian line shape. None of these band profiles are similar to the measured profiles shown in Figure 5.

We have calculated the TDM of the different OH- and OD-stretching transitions simply as the vector defined by: $|\langle v|\vec{\mu}|0\rangle|^2$. The TDM shows significant change in its direction with vibrational excitation, as also observed in a few other molecules.[68−71] The TDM is not located along the OH bond, as one might expect, but for the fundamental transition it is located approximately between the *a*- and *b*-axis. For the vibrational overtones it rotates toward the *a*-axis as v increases. The rotation of the TDM in phenol-d_0 with vibrational excitation is illustrated in Figure 7. Thus the rotational bands are of the a/b hybrid type with more pronounced a-type character as v increases. It is not surprising that the TDM has a different direction for the various transitions as the intensity of these transitions depends on different derivatives of the dipole moment function, whose components along the *a*- and *b*-axis are different.[72] The rotation of the TDM is very similar for phenol-d_5 and for OD-stretching vibrations in the other isotopomers. In Figure 7, we also show the rotational band structure for the OH-stretching transition in phenol-d_0 simulated with the calculated TDM of the fundamental and three vibrational overtones. A Lorentzian profile of 0.1 cm^{-1} width is assumed for each rotational line. The overall width of the bands increase from ~1 cm^{-1} at $T_{rot} = 1$ K to ~3 cm^{-1} at 5 K. The rotational bands are of the a/b hybrid type with more pronounced a-type character as v increases. This variation is much clearer in the rotational profile at 1 K rather than that at 5 K. The effect of this rotation on the band profile is limited, and the direction of the TDM is difficult to determine from experiment, unless the spectra are rotationally resolved.[71] The simulated rotational structure for the other isotopomers is very similar and is not shown. These simulated bands show rotational structure that is not seen in the observed transitions shown in Figure 5 except for $|1>_{OH}$ in phenol-d_5, as we will show.

The lifetime of $|1>_{OH}$ in phenol-d_5 has been reported as 80 ps by the picosecond IR−UV pump−probe experiment.[43] This lifetime corresponds to a 0.07 cm^{-1} broadening of each rotational line, which is comparable to or narrower than the resolution of our IR laser. If IVR is ignored, we can simulate the profile of this band and determine the rotational temperature T_{rot}. In Figure 8 we compare the calculated band profiles of $|1>_{OH}$ in phenol-d_5 at various T_{rot} with the observed band profile. We find that the band profile calculated for $T_{rot} = 0.5$ K is a close match to the observed band. This suggests that the $|1>_{OH}$ state in phenol-d_5 is not coupled to any doorway states or that the involved doorway states are lying very close.

We know that T_{rot} of phenol-d_6 is the same as that of phenol-d_5 because both were measured in the same supersonic jet expansion. It is also reasonable to assume that T_{rot} would be the same for the other two isotopomers. The band profiles calculated assuming $T_{rot} = 0.5$ K are shown in Figure 5 for all four phenol isotopomers and are compared with the observed bands. The calculated band profiles have a width of less than 1 cm^{-1} and are narrower than the observed band shapes. It is clear that the observed overtones are broadened by IVR and that is why we cannot resolve the clear rotational structure.

The broadening due to IVR is consistent with the significantly shorter lifetime of the phenol-d_0 fundamental (14 ps) compared with that of phenol-d_5. In the statistical limit, without specific states to which the excited states are strongly coupled, the IVR rate would be proportional to the state density in the bath. The bath density rapidly increases in going from the fundamental vibrational region to the overtone. If we assume harmonic frequencies, the state density is ~110 states/cm^{-1} in the fundamental region increasing to ~4×10^8 states/cm^{-1} at $v = 4$. The observed bands in Figure 5 clearly show that the bandwidth behavior is far from the statistical limit. This strongly suggests that the band shapes are distorted by the line broadening from relaxation and that the different band shape reflects the difference of the IVR processes including selected resonances which would give rise to multipeak shapes. Page et al. showed that the IVR processes in a typical large molecule, such as benzene, are not at the statistical limit, and specific doorway states in the so-called "tier-model" are important.[73] They found bandwidths in benzene of about 4−10 cm^{-1}, similar to those we find for phenol. More recently, it was found that the IVR of the fundamental transitions of phenol-d_0, -d_1, and -d_5 relied on doorway states and that the widths were dependent also on the strength of the coupling to these doorway states.[43,44] In the tier-model, the initially prepared state strongly couples with specific doorway states in the bath. These doorway states subsequently couple with other bath states. We consider this IVR tier-model with regard to our recorded OH- and OD-stretching overtone spectra and try to explain qualitatively the observed change of bandwidth.

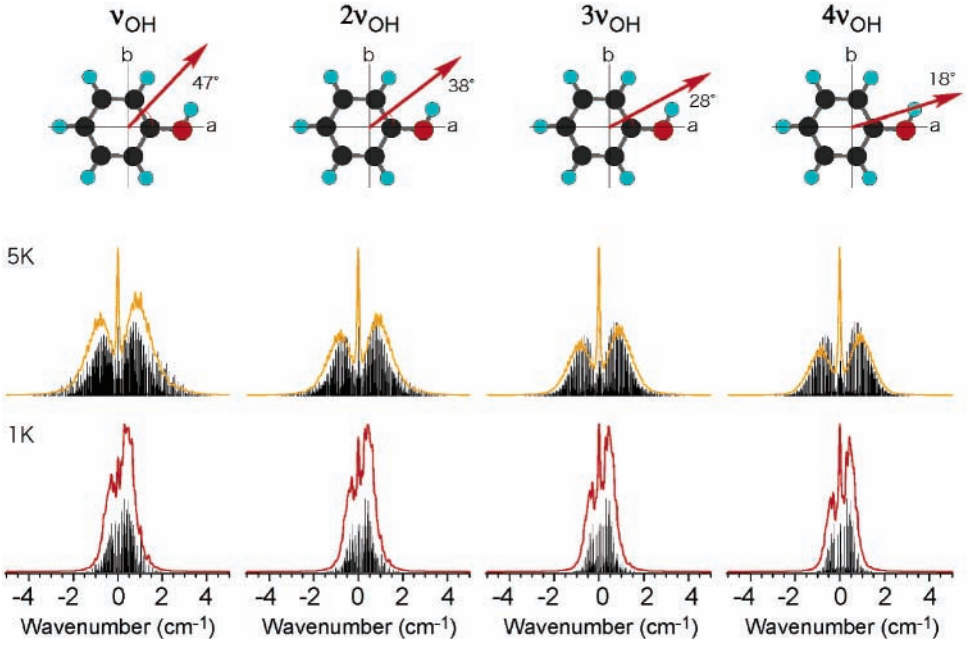

Figure 7. Calculated rotational contours for the fundamental and overtone OH-stretching vibrations in phenol-d_0 simulated at $T_{rot} = 1$ and 5 K. The orientation of the transition dipole moment and its angle with the *a*-axis is indicated.

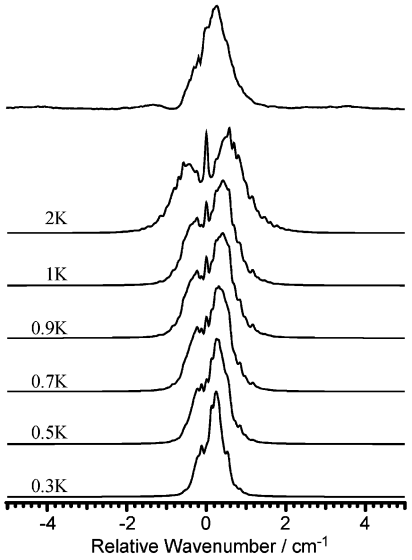

Figure 8. Observed NID spectrum of the OH-stretching fundamental in phenol-d_5 (top trace) and simulated rotational contours for $T_{rot} =$ 0.3, 0.5, 0.7, 0.9, 1, and 2 K with 0.1 cm^{-1} line widths of the individual rotational lines.

An interesting point is that the bandwidth changes somewhat regularly with the vibrational quantum number. In phenol-d_0 and -d_6, the bandwidths decrease with increasing vibrational quantum number, whereas in phenol-d_1 and -d_5, an increasing bandwidth is observed as the quantum number increases. In both phenol-d_0 and -d_6 the same trend is observed despite the bands arising from OH- and OD-stretching transitions, respectively, and a similar trend is observed for phenol-d_5 and -d_1. This suggests that the CH(CD) vibrations are critical to the IVR in OH(OD)-stretching overtones and that the energy separation between the OH(OD)-stretching and CH(CD)-stretching vibrations plays an important role. The significant difference in lifetimes of the fundamental OH-stretching state observed for phenol-d_0 and -d_5 also strongly suggests involvement of CH-stretching states.[43]

Let us assume that the OH-stretching vibration is strongly coupled with a doorway state that includes the CH-stretching vibration. The combination state of CH stretching ($\sim$3000 cm^{-1}) and one of the numerous CC skeletal modes ($\sim$600 cm^{-1}) would have a vibrational frequency of $\sim$3600 cm^{-1}, which can be resonant with the OH-stretching state. Then, the OH-stretching state can be relaxed quickly through this doorway state. This accidental resonance will be less likely the higher the overtone as the OH-stretching vibration has a high anharmonicity and the frequency difference between subsequent OH-stretching transitions decreases. Thus the coupling will be weaker, the IVR rate slower, and the bandwidth narrower. The same explanation is applicable to the IVR in phenol-d_6 and is in agreement with the observed decrease in bandwidth with increased vibrational excitation.

On the other hand, the same accidental resonances are not nearly as likely for the partially deuterated phenols, phenol-d_1 and -d_5. In the former, the CH-stretching states lie higher than the OD-stretching state (Figure 2), and in phenol-d_5, the energy gap between the CD- and OH-stretching vibrations is $\sim$1000 cm^{-1}, which is an infrequent frequency in phenol-d_5. In these two molecules the IVR from the OH- or OD-stretching state might be driven mainly by a number of weakly coupled doorway and/or bath states, and its rate will simply increase with vibrational excitation according to the increase of the density of the states in the bath. Our argument is quite qualitative but does offer an explanation for the systematic change of the bandwidth of phenol and its deuterated isotopomers.

We have attempted to find specific doorway states by looking at combinations of all the vibrational modes.[74] However, at present, it is quite difficult to specify the doorway state on the basis of the theoretical calculations because we cannot calculate these accurately enough. Recall that the bandwidths are at most 10 cm^{-1} and the vibrational states would have to be calculated with sub-cm^{-1} accuracy. This is not possible for molecules of this size, not even for the fundamental harmonic frequencies. Another complication is that vibrational frequencies change with OH-vibrational excitation. The B3LYP calculated harmonic frequencies for the phenol-d_0 and phenol-d_0 in which the OH bond was stretched by an amount equivalent to the average OH bond length displacement at the $\upsilon_{OH} = 3$ vibrationally excited state ($\sim$0.11Å) are compared in Table 3S. Relatively small

changes of 1−2 cm^{-1} are seen for the CH-stretching vibrations, whereas significant changes occur for some of the other vibrational modes making the task of determining theoretically specific doorway states difficult.

Conclusion

We have measured the fundamental and first two OH- and OD-stretching overtone transitions in phenol and its deuterated isotopomers phenol-d_1, -d_5, and -d_6 in a supersonic jet by nonresonant ionization detected spectroscopy. The room-temperature vapor-phase IR and NIR spectra of phenol are also recorded using conventional and photoacoustic spectroscopy. The positions and intensities of the OH-, OD- and CH-overtone transitions are well reproduced by an anharmonic oscillator local mode model. The calculated intensities compare favorably both with absolute intensities measured in the conventional spectra and with relative intensities obtained in the room-temperature photoacoustic spectrum.

Our calculations show that the direction of the transition dipole moment rotates toward the *a*-axis from the fundamental to the third overtone OH(D)-stretching transition. For the fundamental transitions, the angle with the rotational *a*-axis is ∼47°, which decreases to ∼18° for the third overtone. This results in an a/b-type hybrid rotational structure of these OH(D)-stretching transitions. On the basis of the calculated transition dipole moment, we have successfully simulated the narrow OH-stretching fundamental transition in phenol-d_5. We find that the phenol-d_5 fundamental band observed can be modeled well by a rotational temperature of ∼0.5 K and a rotational line width of 0.1 cm^{-1}. This rotational line width is consistent with previous lifetime measurements of this transition and the resolution of our laser. We also calculated the rotational band shape for all other transitions on the basis of the calculated transition dipole moment, the rotational temperature of 0.5 K, and rotational line width of 0.1 cm^{-1}. We find that the observed band shapes are significantly wider than the calculated ones and can only be explained when the bright state is coupled to a few doorway states and that possibly the rotational lines are IVR broadened (tier-model).

In both phenol-d_0 and -d_6, the widths of the band shape decrease with increasing vibrational quantum number, whereas in the partially deuterated phenols phenol-d_1 and -d_5, an increasing bandwidth is observed as the quantum number increases. These results show that the IVR occurs nonstatistically, even in the overtones of a larger polyatomic molecule like phenol, and that the existence of the accidentally resonant doorway states in the bath strongly affects the IVR process. Though we cannot assign the doorway states, our results suggest the contribution of CH- and CD-stretching vibrations in this IVR.

The nonstatistical IVR in overtones of phenol suggests that reaction control via overtone excitation could be possible even for larger polyatomic molecules. Recent progress in light sources suggests that overtone spectroscopy will become more important for reaction control.

Acknowledgment. The authors would like to thank Daryl L. Howard, Richard N. Zare, and Jonathan H. Gutow for helpful discussions. We thank Bryan R. Henry and Michael W. P. Petryk for help with the CARY conventional spectra, which were recorded with their instrument at the University of Guelph. We thank Minako Shinozaki for help with running the calculations on the computer at the Institute for Molecular Science, Okazaki. H.G.K. is grateful to the Japan Society for Promotion of Science for a visiting fellowship, and T.W.R. is grateful to the Foundation for Research, Science and Technology for a Bright Futures Top Achiever Doctoral Scholarship. The Ministry of Education, Culture, Sports, Science and Technology (MEXT) and the Marsden Fund administered by the Royal Society of New Zealand have provided funding for this research.

Supporting Information Available: Two tables with B3LYP/6-311++G(2d,2p) calculated harmonic frequencies, one table with CH and OH bond lengths, one table with the QCISD optimized geometry, one table with calculated CH-stretching intensities; three figures with the room-temperature IR and the NIR spectra in the $\Delta v_{OH} = 4$ and 5 regions. This material is available free of charge via the Internet at http://pubs.acs.org.

References and Notes

(1) Donaldson, D. J.; Tuck, A. F.; Vaida, V. *Chem. Rev.* **2003**, *103*, 4717.
(2) Donaldson, D. J.; Frost, G. J.; Rosenlof, K. H.; Tuck, A. F.; Vaida, V. *Geophys. Res. Lett.* **1997**, *24*, 2651.
(3) Zhang, H.; Roehl, C. M.; Sander, S. P.; Wennberg, P. O. *J. Geophys. Res., [Atmos.]* **2000**, *105*, 14593.
(4) Salawitch, R. J.; Wennberg, P. O.; Toon, G. C.; Sen, B.; Blavier, J. F. *Geophys. Res. Lett.* **2002**, *29*, 1762.
(5) Roehl, C.; Nizkorodov, S. A.; Zhang, H.; Blake, G. A.; Wennberg, P. O. *J. Phys. Chem. A* **2002**, *106*, 3766.
(6) Vaida, V.; Kjaergaard, H. G.; Hintze, P. E.; Donaldson, D. J. *Science* **2003**, *299*, 1566.
(7) Mills, M. J.; Toon, O. B.; Vaida, V.; Hintze, P. E.; Kjaergaard, H. G.; Schofield, D. P.; Robinson, T. W. *J. Geophys. Res.* **2005**, *110*, D08201.
(8) Burkholder, J. B.; Mills, M.; McKeen, S. *Geophys. Res. Lett.* **2000**, *27*, 2493.
(9) Robinson, T. W.; Schofield, D. P.; Kjaergaard, H. G. *J. Chem. Phys.* **2003**, *118*, 7226.
(10) Hintze, P. E.; Kjaergaard, H. G.; Vaida, V.; Burkholder, J. B. *J. Phys. Chem. A* **2003**, *107*, 1112.
(11) Kjaergaard, H. G.; Lane, J. R.; Schofield, D. P.; Robinson, T. W.; Jorgensen, P.; Mills, M. J. Unpublished work, 2006.
(12) Rizzo, T. R.; Crim, F. F. *J. Chem. Phys.* **1982**, *76*, 2754.
(13) Chandler, D. W.; Farneth, W. E.; Zare, R. N. *J. Chem. Phys.* **1982**, *77*, 4447.
(14) Ticich, T. M.; Rizzo, T. R.; Dubal, H. R.; Crim, F. F. *J. Chem. Phys.* **1986**, *84*, 1508.
(15) Sinha, A.; Vander Wal, R. L.; Crim, F. F. *J. Chem. Phys.* **1990**, *92*, 401.
(16) Sinha, A.; Vander Wal, R. L.; Crim, F. F. *J. Chem. Phys.* **1989**, *91*, 2929.
(17) Xing, G.; Wang, X.; Huang, X.; Bersohn, R.; Katz, B. *J. Chem. Phys.* **1996**, *104*, 826.
(18) Zhu, L.; Suto, K.; Fiss, J. A.; Wada, R.; Seidemam, T.; Gordon, R. J. *Phys. Rev. Lett.* **1997**, *79*, 4108.
(19) Chiu, Y.; Fu, H.; Huang, J.; Anderson, S. L. *J. Chem. Phys.* **1994**, *101*, 5410.
(20) Chiu, Y.; Fu, H.; Huang, J.; Anderson, S. L. *J. Chem. Phys.* **1995**, *102*, 1199.
(21) Guettler, R. D.; Jones, G. C., Jr.; Posey, L. A.; Zare, R. N. *Science* **1994**, *266*, 259.
(22) Kreher, C.; Theinl, R.; Gericke, K. H. *J. Chem. Phys.* **1996**, *104*, 4481.
(23) Sinha, A.; Hsiao, M. C.; Crim, F. F. *J. Chem. Phys.* **1990**, *92*, 6333.
(24) Sinha, A.; Hsiao, M. C.; Crim, F. F. *J. Chem. Phys.* **1991**, *94*, 4928.
(25) Sinha, A.; Thoemke, J. D.; Crim, F. F. *J. Chem. Phys.* **1992**, *96*, 372.
(26) Bardeen, C. J.; Yakovlev, V. V.; Wilson, K. R.; Carpenter, S. D.; Weber, P. M.; Warren, W. S. *Chem. Phys. Lett.* **1997**, *280*, 151.
(27) Yakovlev, V. V.; Bardeen, C. J.; Che, J.; Cao, J.; Wilson, K. R. *J. Chem. Phys.* **1998**, *108*, 2309.
(28) Ohmori, K.; Nakamura, A.; Chiba, A.; Amano, K.; Okunishi, A.; Sato, Y. *J. Photochem. Photobio., A* **2001**, *145*, 17.
(29) Omi, T.; Shitomi, H.; Sekiya, N.; Takazawa, K.; Fujii, M. *Chem. Phys. Lett.* **1996**, *252*, 287.
(30) Kjaergaard, H. G.; Howard, D. L.; Schofield, D. P.; Robinson, T. W.; Ishiuchi, S.-i.; Fujii, M. *J. Phys. Chem. A* **2002**, *106*, 258.
(31) Ishiuchi, S.-i.; Shitomi, H.; Takazawa, K.; Fujii, M. *Chem. Phys. Lett.* **1998**, *283*, 243.
(32) Robinson, T. W.; Kjaergaard, H. G.; Ishiuchi, S.-i.; Shinozaki, M.; Fujii, M. *J. Phys. Chem. A* **2004**, *108*, 4420.
(33) Evans, J. C. *Spectrochim. Acta* **1960**, *16*, 1382.

(34) Green, J. H. S. *J. Chem. Soc.* **1961**, 2236.
(35) Bist, H. D.; Brand, J. C.; Williams, D. R. *J. Mol. Spectrosc.* **1967**, *24*, 402.
(36) Lampert, H.; Mikenda, W.; Karpfen, A. *J. Phys. Chem. A* **1997**, *101*, 2254.
(37) Michalska, D.; Zierkiewicz, W.; Bienko, D. C.; Wojciechowski, W.; Zeegers-Huyskens, T. *J. Phys. Chem. A* **2001**, *105*, 8734.
(38) Michalska, D.; Bienko, D. C.; Abkowicz-Bienko, A. J.; Latajka, Z. *J. Phys. Chem.* **1996**, *100*, 17786.
(39) Davidsson, J.; Gutow, J. H.; Zare, R. N. *J. Phys. Chem.* **1990**, *94*, 4069.
(40) Gutow, J. H.; Davidsson, J.; Zare, R. N. *Chem. Phys. Lett.* **1991**, *185*, 120.
(41) Rospenk, M.; Leroux, N.; Zeegers-Huyskens, T. *J. Mol. Spectrosc.* **1997**, *183*, 245.
(42) Rospenk, M.; Czarnik-Matusewicz, B.; Zeegers-Huyskens, T. *Spectrochim. Acta, Part A* **2001**, *57*, 185.
(43) Yamada, Y.; Ebata, T.; Kayano, M.; Mikami, N. *J. Chem. Phys.* **2004**, *120*, 7400.
(44) Yamada, Y.; Mikami, N.; Ebata, T. *J. Chem. Phys.* **2004**, *121*, 11530.
(45) Henry, B. R. *Acc. Chem. Res.* **1987**, *20*, 429.
(46) Kjaergaard, H. G.; Turnbull, D. M.; Henry, B. R. *J. Chem. Phys.* **1993**, *99*, 9438.
(47) Kjaergaard, H. G.; Yu, H.; Schattka, B. J.; Henry, B. R.; Tarr, A. W. *J. Chem. Phys.* **1990**, *93*, 6239.
(48) Dopfer, O.; Muller-Dethlefs, K. *J. Chem. Phys.* **1994**, *101*, 8508.
(49) Rong, Z.; Kjaergaard, H. G. *J. Phys. Chem. A* **2002**, *106*, 6242.
(50) Atkins, P. W.; Friedman, R. S. *Molecular Quantum Mechanics*, 3rd ed.; Oxford University Press: Oxford, U.K., 1997.
(51) Kjaergaard, H. G.; Goddard, J. D.; Henry, B. R. *J. Chem. Phys.* **1991**, *95*, 5556.
(52) Low, G. R.; Kjaergaard, H. G. *J. Chem. Phys.* **1999**, *110*, 9104.
(53) Reddy, K. V.; Heller, D. F.; Berry, M. J. *J. Chem. Phys.* **1982**, *76*, 2814.
(54) Frisch, M. J.; Trucks, G. W.; Schlegel, H. B.; Scuseria, G. E.; Robb, M. A.; Cheeseman, J. R.; Zakrzewski, V. G.; Montgomery, J. A., Jr.; Stratmann, R. E.; Burant, J. C.; Dapprich, S.; Millam, J. M.; Daniels, A. D.; Kudin, K. N.; Strain, M. C.; Farkas, O.; Tomasi, J.; Barone, V.; Cossi, M.; Cammi, R.; Mennucci, B.; Pomelli, C.; Adamo, C.; Clifford, S.; Ochterski, J.; Petersson, G. A.; Ayala, P. Y.; Cui, Q.; Morokuma, K.; Malick, D. K.; Rabuck, A. D.; Raghavachari, K.; Foresman, J. B.; Cioslowski, J.; Ortiz, J. V.; Stefanov, B. B.; Liu, G.; Liashenko, A.; Piskorz, P.; Komaromi, I.; Gomperts, R.; Martin, R. L.; Fox, D. J.; Keith, T.; Al-Laham, M. A.; Peng, C. Y.; Nanayakkara, A.; Gonzalez, C.; Challacombe, M.; Gill, P. M. W.; Johnson, B. G.; Chen, W.; Wong, M. W.; Andres, J. L.; Head-Gordon, M.; Replogle, E. S.; Pople, J. A. *Gaussian 98*, revision 8.7; Gaussian, Inc.: Pittsburgh, PA, 1998.
(55) Larsen, N. W. *J. Mol. Struct.* **1979**, *51*, 175.
(56) Martinez, S. J.; Alfano, J. C.; Levy, D. H. *J. Mol. Spectrosc.* **1992**, *152*, 80.
(57) Portalone, G.; Schultz, G.; Domenicano, A.; Hargittai, I. *Chem. Phys. Lett.* **1992**, *197*, 482.
(58) Sage, M. L. *Isr. J. Chem.* **2004**, *44*, 37.
(59) Rospenk, M.; Czarnik-Matusewicz, B.; Zeegers-Huyskens, T. *Spectrochim. Acta, Part A* **2001**, *57*, 185.
(60) Etzkorn, T.; Klotz, B.; Sorensen, S.; Patroescu, I. V.; Barnes, I.; Becker, K. H.; Platt, U. *Atmos. Environ.* **1999**, *33*, 525.
(61) Broun, E. V. *Opt. Spectrosc.* **1967**, *23*, 301.
(62) Ingold, K. U. *Can. J. Chem.* **1962**, *40*, 111.
(63) Gutow, J. H. Personal communication, 2003.
(64) Rong, Z.; Henry, B. R.; Robinson, T. W.; Kjaergaard, H. G. *J. Phys. Chem. A* **2005**, *109*, 1033.
(65) Kjaergaard, H. G.; Henry, B. R. *Mol. Phys.* **1994**, *83*, 1099.
(66) Kjaergaard, H. G.; Daub, C. D.; Henry, B. R. *Mol. Phys.* **1997**, *90*, 201.
(67) Kjaergaard, H. G.; Bezar, K. J.; Brooking, K. A. *Mol. Phys.* **1999**, *96*, 1125.
(68) Fair, J. R.; Votava, O.; Nesbitt, D. J. *J. Chem. Phys.* **1998**, *108*, 72.
(69) Hurtmans, D.; Herregodts, F.; Herman, M.; Lievin, J.; Campargue, A.; Garnache, A.; Kachanov, A. A. *J. Chem. Phys.* **2000**, *113*, 1535.
(70) Takahashi, K.; Sugawara, M.; Yabushita, S. *J. Phys. Chem. A* **2005**, *109*, 4242.
(71) Konen, I. M.; Li, E. X. J.; Stephenson, T. A.; Lester, M. I. *J. Chem. Phys.* **2005**, *123*, 204318.
(72) Kjaergaard, H. G.; Henry, B. R. *J. Chem. Phys.* **1992**, *96*, 4841.
(73) Page, R. H.; Shen, Y. R.; Lee, Y. T. *J. Chem. Phys.* **1988**, *88*, 4621.
(74) Ishiuchi, S.-i. Ph.D. Thesis, Graduate University for Advanced Study, Okazaki, Japan, 2001.